combustion of fossil fuels, particularly coal. This source is predicted to grow in strength during the early- to mid-twenty-first century (**Figure 5**).

Conclusion

Land–sea exchange processes and fluxes of the bioessential elements are critical to life. In several cases documented above, these exchanges have been substantially modified by human activities. These modifications have led to a number of environmental issues including global warming, acid deposition, excess atmospheric nitrogen deposition, and production of photochemical smog. These issues all have consequences for the biosphere – some well known, others not so well known. It is likely that the developing world, with increasing population pressure and industrial development and with no major changes in agricultural technology and energy consumption rates, will become a more important source of airborne gases and aerosols and materials for river and groundwater systems in the future. This will lead to further modification of land–sea global transfers. The region of southern and eastern Asia is particularly well poised to influence significantly these global transfers.

See also

Aeolian Inputs. Air–Sea Transfer: Dimethyl Sulphide, COS, CS_2, NH_4, Non-methane Hydrocarbons, Organo-halogens. Carbon Cycle. Carbon Dioxide (CO_2) Cycle. Coastal Topography, Human Impact on. Nitrogen Cycle. Ocean Carbon System, Modelling of. Past Climate From Corals. Phosphorus Cycle. Thermohaline Circulation.

Further Reading

Berner EA and Berner RA (1996) *Global Environment: Water, Air and Geochemical Cycles*. Upper Saddle River, NJ: Prentice Hall.

Galloway JN and Melillo JM (eds) (1998) *Asian Change in the Context of Global Change*. Cambridge: Cambridge University Press.

Mackenzie FT (1998) *Our Changing Planet: An Introduction to Earth System Science and Global Environmental Change*. Upper Saddle River, NJ: Prentice-Hall.

Schlesinger WH (1997) *Biogeochemistry: An Analysis of Global Change*. San Diego, California: Academic Press.

Smith SV and Mackenzie FT (1987) The ocean as a net heterotrophic system: Implications from the carbon biogeochemical cycle. *Global Biogeochemical Cycles* 1: 187–198.

Ver LM, Mackenzie FT and Lerman A (1999) Biogeochemical responses of the carbon cycle to natural and human perturbations: Past, present, and future. *American Journal of Science* 299: 762–801.

Vitousek PM, Aber JD, Howarth RW *et al.* (1997) Human alteration of the global nitrogen cycle: Sources and consequences. *Ecological Applications* 7 (3): 737–750.

Wollast R and Mackenzie FT (1989) Global biogeochemical cycles and climate. In: Berger A, Schneider S and Duplessy JC (eds) *Climate and Geo-Sciences*, pp. 453–473. Dordrecht: Kluwer Academic Publishers.

LANGMUIR CIRCULATION AND INSTABILITY

S. Leibovich, Cornell University, Ithaca, NY, USA

doi:10.1006/rwos.2001.0141

Introduction

The surface of a wind-driven sea often is marked by streaks roughly aligned with the wind direction. These streaks, or windrows, are visible manifestations of coherent subsurface motions extending throughout the bulk of the ocean surface mixed layer, extending from the surface down to the seasonal thermocline. These may be regarded as the large scales of the turbulence in the mixed layer. Windrows and their subsurface origins were first systematically studied and described by Irving Langmuir in 1938, and the phenomenon since has become known as Langmuir circulation. The existence of a simple deterministic description making these large scales theoretically accessible distinguishes this problem from coherent structures in other turbulent flows. The theory traces these patterns to a convective instability mechanically driven by the wind waves and currents. Recent advances in instrumentation and computational data analysis have led to field observations of Langmuir circulation of unprecedented detail. Although the body of observational data obtained since Langmuir's own work is mainly qualitative, ocean experiments now can yield quantitative measurements of velocity fields in the near surface region. New measurement

methods are capable of producing data comprehensive enough to characterize the phenomenon, and its effect on the stirring and maintenance of the mixed layer, although the labor and difficulties involved and the sheer complexity of the processes occurring in the surface layer leave much work to be done before this can be said to be accomplished. Nevertheless, the combination of new experimental techniques and a simple and testable theoretical mechanism has stimulated rapid progress in the exploration of the stirring of the ocean surface mixed layer.

Description of Langmuir Circulation

Langmuir circulation takes the ideal form of vortices with axes aligned with the wind, as in the schematic drawing in **Figure 1**. The appearance resembles convective rolls driven by thermal convection, but all evidence indicates that the motions are due to mechanical processes through the action of the wind, as Langmuir originally indicated. At the surface, rolls act to sweep surface water from regions of surface divergence overlying upwelling water into convergence zones overlying downwelling water. Floating material is collected into lines of surface convergence that are visible as windrows.

In confined bodies of water, like lakes and ponds, windrows are very nearly parallel to the wind, and can have a nearly uniform spacing, as shown in **Figure 2**. In the ocean, evidence indicates windrows tend to orient at a small angle to the right of the wind in the Northern Hemisphere; spacing is more

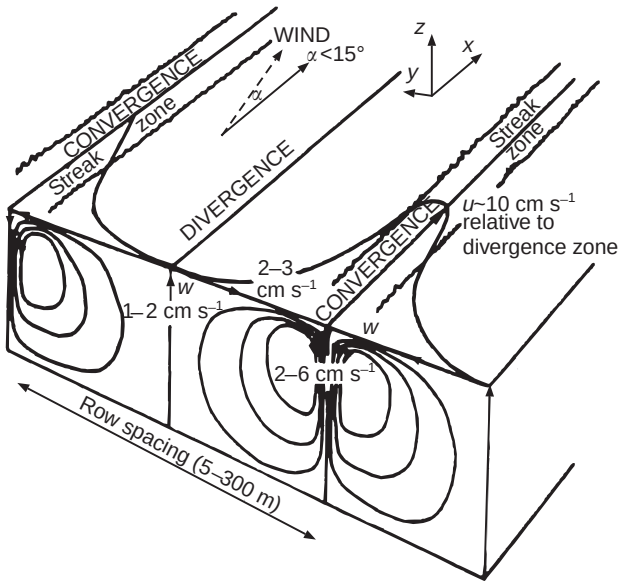

Figure 1 Sketch of Langmuir circulation. (From Langmuir (1938).)

Figure 2 Photograph of windrows in Rodeo Lagoon, California. (From A. Szeri, *Monthly Weather Review*.)

variable and individual windrows can be traced only for a modest multiple of the mean spacing. A windrow may terminate, perhaps due to local absence of surface tracers, or coalesce with an adjacent windrow, or split into two daughter windrows. Thus in the ocean, the general surface appearance is of a network of lines, occasionally intersecting yet roughly aligned with the wind.

Windrows are visible in nature only when both Langmuir circulation and surface tracers are present. In the ocean, bubbles from breaking waves are the most readily available tracers, and Langmuir circulation and bubbles both appear to exist when speeds exceed some threshold. Threshold wind levels are not absolute, since swell, wind duration, fetch, and currents existing before the onset of wind forcing play a role, but windrows are commonly reported in winds of $3\,\mathrm{m\,s^{-1}}$ or more. Tracers other than bubbles may produce windrows with the underlying Langmuir circulation; all forms of flotsam serve. Langmuir first noticed windrows from the deck of a ship in the Sargasso Sea, which contained windrows of *Sargassum*. Organic films on the water surface are compressed in windrows, causing capillary waves to be preferentially damped; in light wind, windrows are thereby made visible as bands of smoother water. Observations in the infrared (see **Figure 3**) reveal windrows due to variation of surface temperature created by Langmuir circulation.

A hierarchy of horizontal scales is observed, with windrow spacing ranging in the ocean from a few meters up to approximately three times the depth of the surface mixed layer. The largest scales are the most energetic and the most persistent, and extend to depths comparable to that of the mixed layer, so

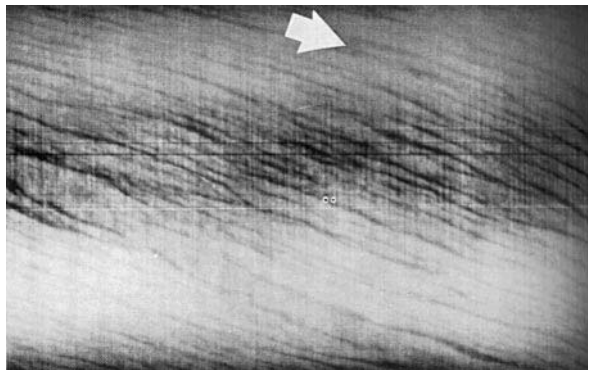

Figure 3 Infrared aerial photograph of thermal streaks in the Pacific. The arrow shows the wind direction. The wind speed is $4\,ms^{-1}$. The image is about 750 m wide (From McLeish, W (1968) On the mechanisms of winslich generation *Deep-Sea Research* 15: 461–469.)

that a cell extending from surface divergence to surface convergence, and from surface to maximum depth of penetration is approximately square. The maximum penetration depth in the open ocean is comparable to the depth of the seasonal thermocline. Langmuir reported the penetration depth in Lake George to be comparable to the epilimnion when the lake was stratified, and believed the epilimnion depth to be created by the mixing caused by the wind-driven convective motion. It is not yet clear whether the seasonal thermocline location is fixed by the scale of Langmuir circulation, or whether the penetration depth of the circulation is limited by the strong buoyancy at the thermocline acting like a bottom, although the latter seems more likely. In shallow water, the seabed or lake floor of course fixes the maximum penetration depth. While horizontal scales of up to three times the mixed layer depth are reported, even larger scales may exist that have not been detected in experiments.

The smaller scales are advected and presumably eventually swept up by the largest scales. If a fixed number of permanent surface markers is used, as in some experiments in which computer cards were released to serve as markers, the larger scales ultimately become more prevalent. Most observations depend on Lagrangian tracers, in particular bubbles with definite lifetimes that are continually but episodically created. The regeneration of bubbles on the surface between the large scale windrows permits the smaller scales to be seen.

The largest observed windrow scales consolidate in about 20 minutes after a shift in wind direction or in cases of sudden wind onset. This appears to establish the formation time, at least that required to sweep surface material into windrows. The largest windrow scales in the Pacific have been observed to persist for hours.

Downwelling speeds below windrows are substantially higher than upwelling speeds occurring below surface divergences. Furthermore, the down-wind surface speed is larger in windrows than between them. Although this has not often been quantified, it appears that the speed increases in surface jets are comparable to the maximum downwelling speeds.

Theory

Theory promulgated in the 1970s has influenced experiments addressing Langmuir circulation. The theory most commonly utilized, and now commonly referred to as Craik–Leibovich theory after its originators, begins with Langmuir's conclusion that the cellular motion bearing his name derives from the wind. Wind blowing over a water surface has two simultaneous consequences: currents are generated as horizontal momentum is transmitted from wind to water; and waves are generated on the water surface due to an instability of the air–sea interface under wind shear.

A detailed treatment of the shear flow in the presence of wind waves is not feasible. The eddy turnover timescale (the time required for a fluid particle to traverse the convective cell) in Langmuir circulation is on the order of tens of minutes. Surface waves have a substantially shorter timescale. Wind-driven water waves can be thought of as comprised of the superposition of wavelets with a continuous range of wavelengths and frequencies, and the amplitudes of waves in a given band of wavelength or frequency can be characterized by an energy spectrum. For the Pierson–Moskowitz empirical wind wave spectrum, the waves at the peak of the spectrum of a wind-driven sea under wind speed U have period approximately $7U/g$. This is a typical value for the energetic part of the wind wave spectrum. For wind speeds leading to observable Langmuir circulation, a characteristic peak wave period is of the order of 5–7 s. Averaging over the waves is therefore useful. Surface gravity waves are approximately irrotational, and orbital speeds near the surface are an order of magnitude larger than the mean speeds in the current system. Although a wind-driven wave field is complex, and generally must be treated probabilistically, the theory depends only on averaged effects due to the net mass drift caused by the waves, and this can often be computed.

Wave Effects: The Stokes Drift

Nonbreaking surface gravity waves have small slopes, and produce a small (second order in wave slope) mean mass motion in the direction of wave propagation. This net water motion is known as the Stokes drift. If $\mathbf{u}_w$ is the Eulerian velocity due to the water waves, the Stokes drift velocity $\mathbf{u}_s$ is approximately given by eqn [1], where the angle brackets represent an average over time.

$$\mathbf{u}_s = \left\langle \int^t \mathbf{u}_w \, dt \bullet \nabla \mathbf{u}_w \right\rangle \qquad [1]$$

An acceptable averaging time to calculate Stokes drift is a modest multiple of the wave period associated with the peak frequency of the energy spectrum. Provided the currents are small compared to the wave orbital speeds, as is usually assumed in the ocean, then the net mass drift due to waves can be approximated by this formula. If the surface wave characteristics can be associated with specified wind fields — for example, if the wave spectrum is measured, or computed by a wave forecasting model, or if it is assumed to follow a standard empirical wave spectrum — then the Stokes drift can be calculated using eqn [1]. The form of the vertical variation will depend on the spectrum, and the resulting functional form will depend on two parameters, the surface value of the drift, U_s, and a length scale, l, representing the characteristic decay depth of the drift. For example, for a small-amplitude monochromatic surface gravity wave with wavelength λ and amplitude a, the Stokes drift velocity is given by eqn [2], where x_3 is the coordinate measured vertically upward from the mean free surface.

$$|\mathbf{u}_s| = U_s \exp(x_3/l), \qquad U_s = \frac{2\pi a^2}{\lambda}\sqrt{\frac{2\pi g}{\lambda}}, \quad l = \frac{\lambda}{4\pi} \qquad [2]$$

In the absence of swell, the direction of the drift is parallel to the wind.

Langmuir Force

Assuming the surface waves can be approximated as irrotational and have orbital speeds large compared to current speeds, averaging yields an apparent extra force on the averaged motion equal to $\mathbf{u}_s \times \boldsymbol{\omega}_a$, where $\mathbf{u}_s$ is the Stokes drift velocity associated with the wave motion, and $\boldsymbol{\omega}_a$ is the averaged absolute vorticity of the water body. The apparent extra force captures mean effects of the wave–current interaction. It has been called the vortex force in the literature, although it might be more appropriate to call it the Langmuir force, which is the term adopted here. The mean Lagrangian velocity, or mass drift, of a fluid particle at position $\mathbf{x}$ at time t exceeds the mean Eulerian velocity of the water by $\mathbf{u}_s$. If the system is referred to a frame rotating with constant angular velocity vector $\boldsymbol{\Omega}$, then the Langmuir force $\mathbf{F}_L$ is given by eqn [3].

$$\mathbf{F}_L(\mathbf{x}, t) = u_s(\mathbf{x}, t) \times (2\boldsymbol{\Omega} + \boldsymbol{\omega}(\mathbf{x}, t)) \qquad [3]$$

where $\boldsymbol{\omega} = \operatorname{curl} \mathbf{u}$. Note that this quantity has dimensions of a force per unit mass. Here $\mathbf{u}$ is the Eulerian mean velocity as seen in the rotating frame, and so $\boldsymbol{\omega}$ is the relative mean vorticity. The full instantaneous velocity field includes fluctuations due turbulence as well as waves, and so the wave-averaged mean velocity filters out not only the waves but also turbulence with timescales comparable to or less than the averaging time. The Boussinesq equations for momentum and temperature, when averaged over a timescale of several wave periods, are eqns [4]–[6].

$$\frac{\partial \mathbf{u}}{\partial t} + \mathbf{u} \bullet \nabla \mathbf{u} + 2\boldsymbol{\Omega} \times \mathbf{u} = -\frac{1}{\rho}\nabla \pi + \beta g (T - \bar{T})\mathbf{e}_3 + \mathbf{u}_s \times (2\boldsymbol{\Omega} + \boldsymbol{\omega}) + \mathscr{F} \qquad [4]$$

$$\frac{\partial T}{\partial t} + (\mathbf{u} + \mathbf{u}_s) \bullet \nabla T = \mathscr{H} \qquad [5]$$

$$\nabla \bullet \mathbf{u} = 0 \qquad [6]$$

In these equations, π is a modified pressure including mean wave effects, centripetal force 'potential' and hydrostatic pressure variations; T is the water temperature; $\bar{T}$ is a reference temperature field that may depend on time and depth; $\mathbf{e}_3$ is a unit vector pointing vertically upward; $\mathscr{F}$ and $\mathscr{H}$ represent the divergence of momentum and heat fluxes, respectively, due to the unresolved turbulent scales. The rectified effects of the waves are represented by the appearance of the Stokes drift in the Langmuir force and in the advection of the scalar T. If other scalar quantities, such as salt concentration, are included, they are governed by equations of the same form as that for T. With suitable subgrid models for $\mathscr{F}$ and $\mathscr{H}$, these equations can be used to compute the motions, including those with turbulent fluctuations having timescales large compared to a wave period. The principal theoretical development is the incorporation of residual wave effects, the Langmuir force and scalar advection augmented by the Stokes

drift velocity. Without these additions, the governing equations are the same as conventional models not accounting for surface waves.

The simplest closure models are the assumptions of constant eddy viscosity, ν_T, and eddy diffusity of heat, κ_T, yielding $\mathscr{F} = \nu_T \nabla^2 \mathbf{u}$ and $\mathscr{H} = \kappa_T \nabla^2 T$. All analytical work done addressing the stability of the mean motion assumes this form, as does most of the computational work on Langmuir circulation.

The discussion so far has been predicated on the existence of wind stress to produce currents and surface waves. Currents due to other causes may exist for a time in the absence of wind. The same is true of surface waves, which may be generated in distant locations and propagate to the region of interest. The Langmuir force continues to exist, and under suitable conditions—especially when the angle between the Stokes drift and current is small—Langmuir circulation may result. Thus the details of the current and wave fields must be known, and scalings based solely on wind or Stokes drift may be misleading.

Scaling

Despite the disclaimer of the previous paragraph, reported Langmuir circulation appears to be confined to situations driven by local wind stress. The motion will depend on the magnitude and (if Coriolis effects apply) direction of the applied wind stress, $\boldsymbol{\tau}$; sea state as prescribed by $\mathbf{u}_s$; the prevailing density stratification; surface thermal conditions; water depth, or specification of conditions of current, temperature, and salinity below the mixed layer; the Coriolis acceleration, which depends on latitude; and initial conditions.

The wind stress is clearly a primary factor; it provides a unit for speed, the friction velocity $u_* = \sqrt{|\boldsymbol{\tau}|/\rho}$, where $\boldsymbol{\tau}$ is the wind stress and ρ is the water density. Several length scales appear, and the choice of unit of length, d, will depend on circumstances. Since observations in the ocean and in stratified lakes indicate the importance of the depth of the seasonal thermocline, it provides a natural choice when it can be defined. Other choices replace this when a strong thermocline does not exist.

Clearly, the range of questions that may be encountered is extensive, and the parameter space encompassing them is too large for a general discussion. The most elementary situation producing Langmuir circulation, however, is that of a nonrotating layer of water of uniform density with finite depth (either to a solid bottom or to strong thermocline that strongly inhibits vertical motion) under the action of a wind of unlimited fetch and duration and with constant speed and direction, producing a sea state with known Stokes drift. With u_* as the unit for speed and d the unit for length, the unit for time is d/u_*, and the problem then depends on the dimensionless parameters U_s/u_*, and l/d, and a parameter characterizing $\mathscr{F}d/u_*^2$. The latter depends on how $\mathscr{F}$ is modeled. If a constant eddy viscosity is used, then the appropriate parameter is Re_*^{-1}, where $Re_* = u_* d/\nu_T$ is the Reynolds number based on eddy viscosity. The designation Re_* can serve as a placeholder for the parameter appropriate for the choice of model. Thus the simplest problem depends on three dimensionless parameters, although, if the motion is restricted to be invariant in the wind direction, the parameter space can be reduced by one. For each additional physical effect, one more parameter is added to the list. For example, if rotation effects are added, the parameter $|\boldsymbol{\Omega}|d/u_*$, an inverse Rossby number, is needed.

For the most elementary case, the velocity vector in the water column is given by $\mathbf{u} = u_* \boldsymbol{\phi}(\mathbf{x}/d, td/u_*, U_s/u_*, l/d, Re_*)$, where $\boldsymbol{\phi}$ is a dimensionless vector-valued function of its arguments. For fixed position and time, the motion depends on the three fixed dimensionless parameters. If the dependence on Re_* and l/d is weak, hypotheses about how $\boldsymbol{\phi}$ depends on U_s/u_* suggest ways to scale experimental data. For example, if the dependence is on the square root, then $\mathbf{u}$ is directly proportional to U_s. If the dependence is linear, then $\mathbf{u}$ is directly proportional to $\sqrt{u_* U_s}$. Both of these scalings have been tried for field data, without conclusive results. In fact, constant eddy viscosity simulations using eqns [4] and [6] fail to indicate a simple functional dependence of $\boldsymbol{\phi}$ on its parameters.

Instability

If all motions are due to wind and perhaps buoyancy forcing, and the wind stress, sea state, and thermal boundary conditions are independent of horizontal position, the theoretical model has exact solutions independent of horizontal position. The natural mechanical conditions to impose in such cases is that of a constant surface stress in a given direction, and, if waves are present, a Stokes drift velocity parallel to the applied stress. These solutions describe flows with no vertical motion and no patterns on the surface. Such flows therefore may be described as featureless.

These exact solutions can be unstable, however, and patterns can develop as a consequence. In the absence of wave effects $\mathbf{u}_s$ and $\mathbf{F}_L$ both vanish, and roll instabilities leading to parallel lines of surface convergence can arise in two physically distinct ways. If the Coriolis acceleration is retained and

thermal effects are ignored, the featureless flow is the well-known stress-driven Ekman layer, and it is unstable for sufficiently large wind stress. (The same problem without Coriolis effects yields plane Couette flow, which is stable.) If thermal effects are accounted for and the water is cooled from above, the motion is unstable for sufficiently large cooling rates.

In the absence of both Coriolis and thermal effects, the motion without surface waves is stable for any value of the surface stress. If waves are present, the action of the Langmuir force causes the flow to be unstable when the applied stress exceeds a threshold value. The preferred instability mode consists of rolls parallel to the wind direction.

If Coriolis accelerations and Langmuir force are simultaneously considered for typical oceanic conditions, the flow instability is close to that found for nonrotating case, and therefore is dominated by the Langmuir circulation mode. The effect of Coriolis acceleration in this case is mainly to shape the underlying featureless flow, and thereby to cause the rolls to have axes oriented to the right of the wind (in the Northern Hemisphere). Similarly, under typical wind conditions in thermally unstable conditions, the Langmuir circulation instability mode dominates thermal instability.

Langmuir circulation requires the generation of coherent vorticity in the wind (streamwise) direction. The mechanism of the Langmuir force can be seen by a simple geometric argument. Ignore Coriolis acceleration and density stratification. This would be appropriate, for example, when considering small bodies of water, such as New York' Lake George in which Langmuir conducted his extensive experiments, after seasonal overturning of the epilimnion. The equation for mean vorticity $\boldsymbol{\omega}$ is then (since $\nabla \bullet \mathbf{u}_s = 0$) given by eqn [7].

$$\frac{\partial \boldsymbol{\omega}}{\partial t} + (\mathbf{u} + \mathbf{u}_s) \bullet \nabla \boldsymbol{\omega} = \boldsymbol{\omega} \bullet \nabla (\mathbf{u} + \mathbf{u}_s) + \nu_T \nabla^2 \boldsymbol{\omega} \quad [7]$$

The long downwind extent of windrows in these circumstances suggests the motions can be idealized as independent of wind direction, and the Stokes drift is parallel to the wind. In this case, and in all cases, the wind supplies vorticity to the water column, but only in the crosswind direction. Now suppose this featureless solution is perturbed by a slight increase in the windward component of velocity, as indicated in **Figure 4**. This generates vertical vorticity of opposite signs on either side of the velocity maximum. This vorticity is rotated by the Stokes drift to produce streamwise vorticity components as shown. This could be a transient feature. The sense of the streamwise vorticity, however, is to produce a convergence near the surface centered on the line through the velocity maximum, and downwelling motion below this line. In the absence of viscosity, this accelerates the fluid at the convergence line, amplifying the original perturbation. This feedback, provides a mechanism for instability, and this picture is confirmed by detailed computation.

The assumption of streamwise invariance implies that no streamwise vorticity is produced by the

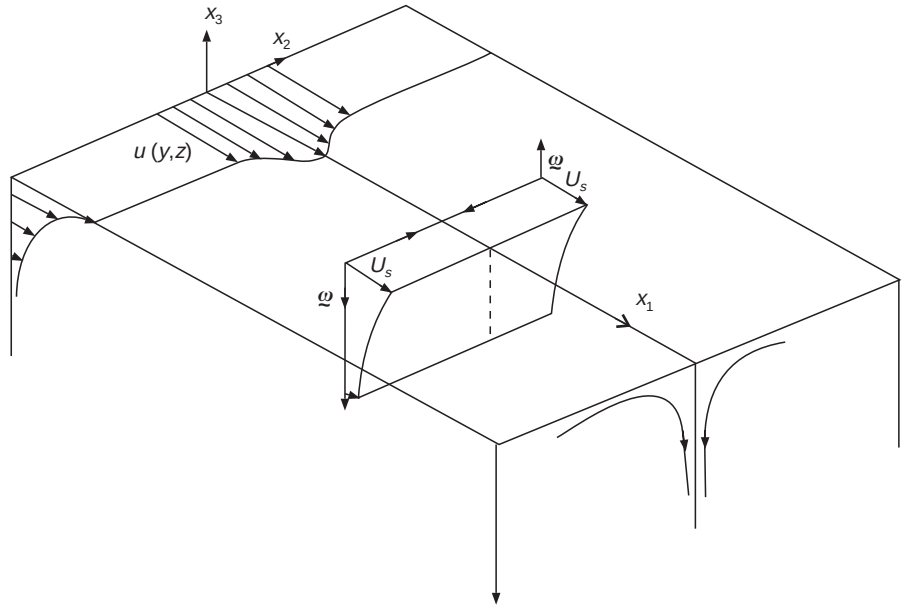

Figure 4 Sketch illustrating instability mechanism.

Eulerian shear – with streamwise invariance of the mean flow, generation of mean streamwise vorticity requires Stokes drift. This may be seen directly from the streamwise component of [7]. If the wind stress is in the x_1-direction, with x_3 oriented vertically upward from the mean free surface, then x_2 will be crosswind in a right-handed (x_1, x_2, x_3) coordinate system with unit vectors $(\mathbf{e}_1, \mathbf{e}_2, \mathbf{e}_3)$. Then $\mathbf{u}_s = U_s(x_3)\mathbf{e}_1, \partial/\partial x_1 = 0$, and the streamwise component of vorticity, $\boldsymbol{\omega}_1$ satisfies eqn [8].

$$\frac{\partial \boldsymbol{\omega}_1}{\partial t} + \frac{\partial u_2 \boldsymbol{\omega}_1}{\partial x_2} + \frac{\partial u_3 \boldsymbol{\omega}_1}{\partial x_3} = \boldsymbol{\omega}_3 \frac{\partial U_s}{\partial x_3} + \nu_T \left(\frac{\partial^2 \boldsymbol{\omega}_1}{\partial x_2^2} + \frac{\partial^2 \boldsymbol{\omega}_1}{\partial x_3^2} \right) \quad [8]$$

Suppose the motion is periodic in the x_2 direction, or that it decays as $|x_2| \to \infty$. Multiplying by $\boldsymbol{\omega}_1$ and integrating over the water depth and over a period in the x_2 direction in the first case or all x_2 in the second, implies eqn [9].

$$\frac{\partial}{\partial t} \int\int \tfrac{1}{2}\boldsymbol{\omega}_1^2 \, dx_2 \, dx_3 = \int\int \boldsymbol{\omega}_1 \boldsymbol{\omega}_3 \frac{\partial U_s}{\partial x_3} dx_2 \, dx_3 - \nu_T \int\int \sum_{j=2}^{3} \left(\frac{\partial \boldsymbol{\omega}_1}{\partial x_j} \right)^2 dx_2 \, dx_3 \quad [9]$$

The second term on the right is the dissipation of the streamwise component of enstrophy, and the first term is its production rate. Production vanishes and streamwise vorticity decays in the absence of Stokes drift. This consequence of streamwise invariance is an exact result for the instantaneous motion; the presence of waves in the instantaneous motion introduces streamwise variations, and the Stokes drift represents the residual effect of these variations in the wave-averaged equations permitting the development of averaged streamwise vorticity.

It is not possible to survey details of instability characteristics for the various cases relevant to the ocean. Qualitatively, however, it can be said that growth rates are consistent with the observed formation rates of Langmuir circulation. In the absence of Coriolis acceleration and stratification, the most unstable mode is in the form of rolls parallel to the wind, and growth is monotonic in time, so the rolls are stationary. When Coriolis acceleration is significant, the underlying featureless flow has a surface velocity to the right of the wind, and the most unstable mode takes an intermediate angle between this and the direction of the wind stress. The growth rates are slightly reduced compared to the comparable problem in the absence of Coriolis effects. The rolls are no longer stationary, but travel normal to their axes, and to the right of the wind.

Only modest wind speeds are required to cause instability in these ways. The unstable character of the ocean under typical winds suggests that perturbations due to a variety of sources, such as breaking waves, grow and reach finite amplitudes. Computer simulations using eqn [4] supports this picture.

Field Observations

New instrumentation, new measurement techniques, and improved data analysis capabilities have clarified the nature of Langmuir circulation. The new methods include greatly improved current meters and sonar methods. Sonars image microbubbles that have a virtually ubiquitous presence in the upper few meters of the ocean. These bubbles are organized by Langmuir circulation; bubble clouds collected by the surface converging motion and carried to form plumes by the downwelling beneath

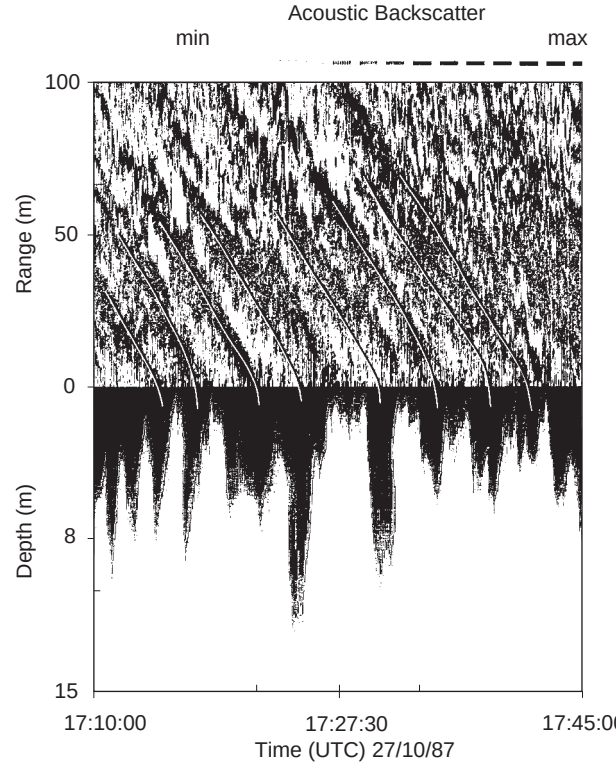

Figure 5 Simultaneous sonar images of windrows and bubble plumes. The upper picture shows bands of scatterers, and the lower picture shows bubble plumes below the bands, over a period of 35 min. From Zedel L and Farmer DM (1991) Organized structures in subsurface bubble clouds: Langmuir circulation in the upper ocean. *Journal of Geophysical Research* 96 (5): 8895.

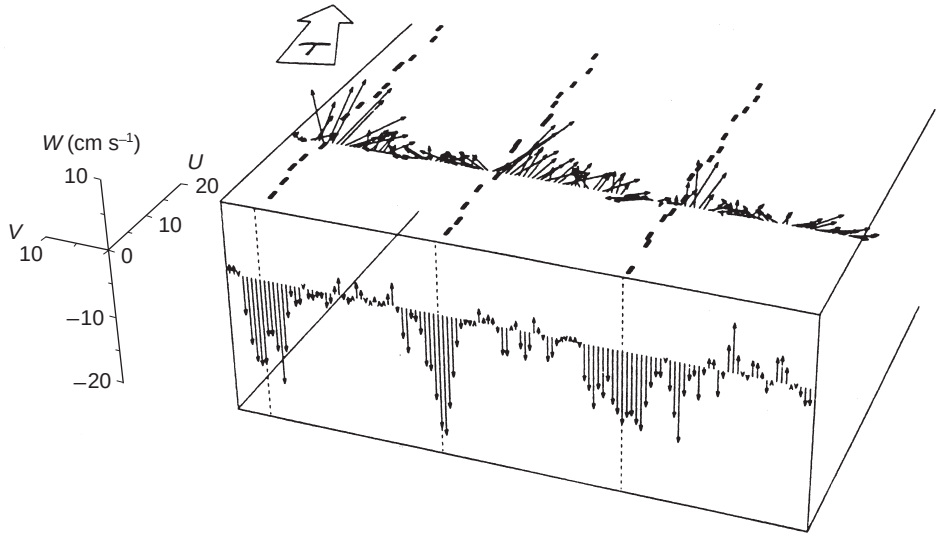

Figure 6 Data from a 50 m deep mixed layer in the Pacific. See text for description. (From Weller RA and Price JF (1988).)

windows, produce strong sonar returns. The intensity of sonar returns permit Langmuir circulation to be visualized in extended regions of the ocean. Doppler sonar can be used to measure speeds in the current system.

Bubble plumes are found to extend to depths of several meters, often up to 10 to 12 m, below windrows. Since the micrometer-sized air bubbles providing the best sonar return signal go into solution and may disappear at depths of this order if the vertical motion is not large, the depth of these plumes provides a lower-bound estimate of the strength of the downwelling motion. **Figure 5** shows an example in which bubbles are organized into bands by Langmuir circulation, and plumes are formed beneath these bands.

A quite remarkable set of measurements taken in 1982 is summarized in **Figure 6**. The data were taken by a string of current meters in a mixed layer about 50 m deep. Velocity measurements are shown near the surface and at 23 m depth, about halfway down from the surface to the base of the mixed layer. Tracks on the surface schematically indicate the disposition of computer cards distributed on the surface to provide visual markers of windrows, which lie about 15° to the right of the wind. The presence of surface jets is indicated, with maximum values of about 20 cm s^{-1}. Surprisingly, the downwelling speeds at 23 m are also about 20 cm s^{-1}. Data taken at other times also produced downwelling speeds from 20 to 30 cm s^{-1} at mid-depth in the mixed layer. These large events occurred intermittently, with less impressive activity, on the order of half as intense, occurring at other times. During these observations, the wind speeds were of the

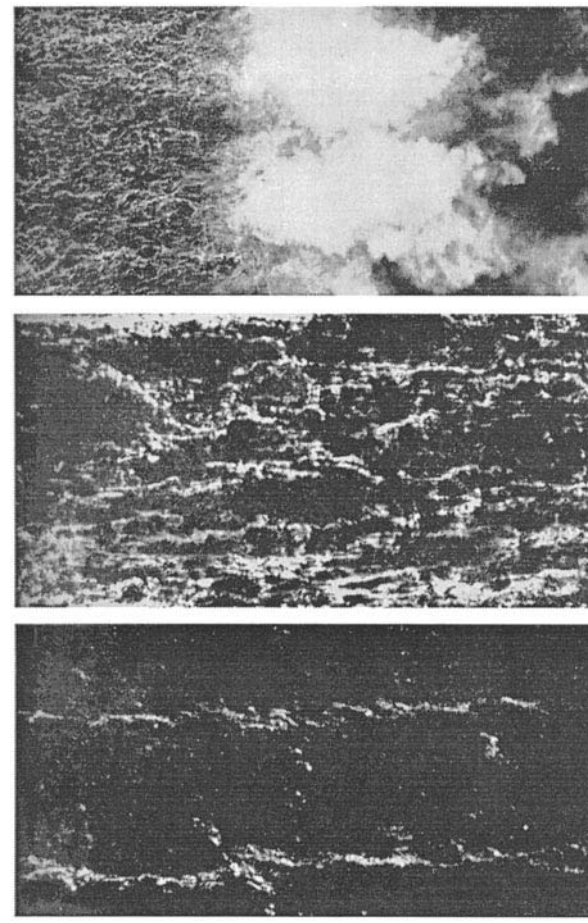

Figure 7 Sulfer powder released from an aircraft and drawn into bands by Langmuir circulation at time of (top to bottom) deployment, 1.5 minutes after, and 20 minutes after. Photograph widths are about 40 m and wind speed is 6 ms^{-1} (From McLeish W (1968) On the mechanisms of wind slide generation *Deep-Sea Research* 5: 461–469.)

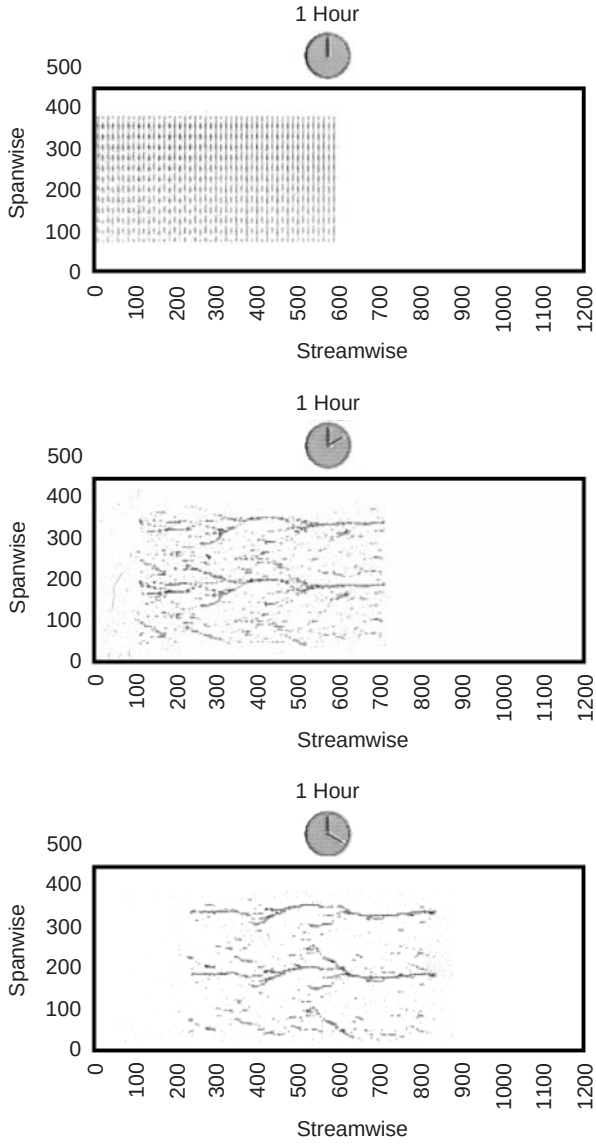

Figure 8 Computer simulation of surface tracers in Langmuir circulation. Compare with **Figure 7**.

order of 8–18 m s^{-1}. Downwelling was observed to be as large as 3 cm s^{-1} under winds as light as 1.5 m s^{-1}.

The process of flotsam collection by Langmuir circulation is shown in **Figure 7**. Sulfur powder was spread along a line across the wind, and appears in an aerial photograph as the light blob in the upper panel immediately afterward. The second and third panels show the disposition of the dust after 1.5 min and 20 min, respectively. Surface tracers advected by the flow produced by a computer simulation of [4] and [6], with a Smagorinsky turbulence subgrid scale closure model is shown in **Figure 8**. Simulated times are indicated by the clock. Note the similarity to **Figure 7**. Large eddy simulation models of Langmuir circulation are now available.

Langmuir circulation is now well-established as an important mechanism, affecting mixing and dispersion in the upper ocean and providing an important dynamical link between the wind-wave field and the development of the mixed layer

See also

Breaking Waves and Near-surface Turbulence. Bubbles. Dispersion in Shallow Seas. Upper Ocean Mixing Processes. Upper Ocean Time and Space Variability. Wind and Buoyancy-forced Upper Ocean.

Further Reading

Langmuir I (1938) Surface motion of water induced by wind. *Science* 87: 119–123.

Leibovich S (1983) The form and dynamics of Langmuir circulation. *Annual Review of Fluid Mechanics* 15: 391–427.

McWilliams JC, Sullivan PP and C-H Moerig (1997) Langmuir turbulence in the ocean. *Journal of Fluid Mechanics* 334: 1–30.

Phillips OM (1977) *The Dynamics of the Upper Ocean*, 2nd edn. Cambridge: Cambridge University Press.

Pollard RT (1977) In: Angel M (ed.) *A Voyage of Discovery: G. Deacon 70th Anniversary Volume Re.* 235–251. Oxford: Pergamon.

Simecek-Beatty D, Lehr WJ, Lai R and Overstreet R (2000) Langmuir circulation and Oil Spill modelling. *Spill Science and Technology Bulletin* 6(3–4): 207–279.

Skyllingstad ED and Dengo DW (1995) An ocean large-eddy simulation of Langmuir circulation and convection in the surface mixed layer. *Journal of Geophysical Research* 100: 8501–8521

Thorpe SA (1985) Small-scale processes in the upper ocean boundary layer. *Nature* 318: 519–522.

Weller RA and Price JF (1988) Langmuir circulation within the oceanic mixed layer. *Deep-Sea Research* 35: 711–747.